Proceedings of the ASME 2010 3rd Joint US-European Fluids Engineering Summer Meeting and 8th International Conference on Nanochannels, Microchannels, and Minichannels
FEDSM-ICNMM2010
August 1-5, 2010, Montreal, Canada

FEDSM-ICNMM2010-31069

SECOND LAW ANALYSIS FOR EXTENDED GRAETZ PROBLEM INCLUDING VISCOUS DISSIPATION IN MICROTUBES

Arman Sadeghi
Ph.D. Student of Mechanical Engineering
Sharif University of Technology, Tehran, Iran

Mostafa Baghani
Ph.D. Candidate of Mechanical Engineering
Sharif University of Technology, Tehran, Iran

Mohammad Hassan Saidi*
Professor of Mechanical Engineering
Sharif University of Technology, Tehran, Iran, P.O. Box: 11155-9567

ABSTRACT

The entropy generation rate has become a useful tool for evaluating the intrinsic irreversibilities associated with a given process or device. This work presents an analytical solution for entropy generation in hydrodynamically fully developed thermally developing laminar flow in a microtube. The rarefaction effects as well as viscous heating effects are taken into consideration, but axial conduction is neglected. Using fully developed velocity profile, the energy equation is solved by means of integral transform. The solution is validated by comparing the local Nusselt numbers against existing literature data. From the results it is realized that the entropy generation decreases as Knudsen number increases, while the effect of increasing values of Brinkman number and the ratio of Brinkman number to dimensionless temperature difference is to increase entropy generation. The average entropy generation number over the cross section of channel increases with increasing values of axial coordinate, until it reaches a constant value at fully developed conditions.

Keywords: Microtube; Graetz problem; Slip flow; Viscous dissipation; Knudsen number; Entropy generation; Bejan

1 INTRODUCTION

Transport phenomena at the microscale reveal many features that are not observed in the macroscale devices. Consequently, fundamental issues related to fluid flow and heat transfer in microchannels need to be resolved for efficient design of microfluidic devices. From a great deal of research, it is clear that continuum analyses are unable to predict gas flow properties in micronsize devices. An experimental investigation of gas flow in channels of 100 μm wide and ranging in depth from 0.5 to 20 μm has been performed by Harley et al. [1] using nitrogen, helium and argon gases. They found that correlations based on classical assumptions cannot predict flow characteristics in microchannels. An experimental investigation was carried out by Araki et al. [2] to study frictional characteristics of nitrogen and helium flows in microchannels with hydraulic diameter range of 3-10 μm. They concluded that the frictional resistance of gas flow in microchannels is smaller than that in the conventional-sized channels.

In rarefied gas flow, the failure of the continuum description is quantified by the Knudsen number, defined as the ratio of the mean free path of gas molecules λ to the channel hydraulic diameter D_h. Based on a definition given by Beskok and Karniadakis [3], gas flow can be classified as one of four regimes according to its Knudsen number. In the slip flow regime which corresponds to $10^{-3} \leq Kn \leq 0.1$, deviations from the state of continuum are relatively small and the Navier-Stokes equations are still valid. The rarefaction effect can be modeled through the partial slip at the wall using slip boundary conditions which can be determined using kinetic theory of gases. The measured friction factors obtained by Harley et al. [1] and Araki et al. [2] matched well with the theoretical predictions assuming fully developed first order slip flow.

The analytical study of internal slip flow has been confined to simple geometries. Kennard [4] studied slip flow in the circular tube and parallel plate channel. Ebert and Sparrow [5] performed an analysis to determine the velocity and pressure drop characteristics of slip flow in rectangular and annular ducts. More recently Duan and Muzychka [6] have performed an analytical analysis to describe fully developed laminar flow in elliptical microchannels. All the results in [4-6] show that

* Corresponding author, Tel: +98 21 66165522; Fax: +98 21 66000021
E-mail address: Saman@sharif.edu

rarefaction effect decreases pressure drop in microchannels with respect to conventional channels for a given mass flow rate.

Also several research works have been undertaken to study heat transfer characteristics of rarefied gas flow in microchannels. Zhu et al. [7] performed a theoretical analysis of heat transfer between two unsymmetrically heated parallel plates with microspacing in the slip flow regime. The influences of the Knudsen number and the accommodation coefficients on the temperature profile and the heat transfer characteristics were determined. Aydin and Avci [8,9] theoretically investigated the steady, laminar, fully developed forced convection in a microtube and microduct between two parallel plates for both boundary conditions of constant wall temperature and constant wall heat flux. Duan and Muzychka [10] have studied heat transfer characteristics of hydrodynamically and thermally fully developed laminar rarefied gas flow in annular microducts with constant wall heat fluxes. Both hydrodynamically and thermally fully developed laminar slip flow forced convection in a rectangular microchannel under H1 boundary condition was studied by Ghodoossi and Egrican [11], using integral transform method.

The problem of hydrodynamically fully developed and thermally developing flow in a channel, with the assumptions of steady and incompressible flow, constant fluid properties and negligible energy dissipation and streamwise conduction effects is known as the Graetz problem, the one which originally solved this problem for a circular tube [12]. The Graetz problem for a microchannel has gained interest because of its fundamental importance in microfluidic problems such as the analysis and design of micro heat exchangers. Barron et al. [13] and Ameel et al. [14] have extended the Graetz problem to slip flow through a microtube with uniform temperature and uniform heat flux boundary conditions, respectively. Thermally developing laminar slip flow forced convection in rectangular microchannels has been studied by Yu and Ameel [15] by applying a modified generalized integral transform technique to solve the energy equation, assuming hydrodynamically fully developed flow.

Another parameter at microscale which should be taken into consideration is the viscous dissipation effects. Viscous dissipation features as a source term in the fluid flow due to the conversion of kinetic motion of the fluid to thermal energy and causes the variation in the temperature distribution. The effects of viscous dissipation on the temperature field and ultimately on the friction factor have been investigated by Koo and Kleinstreuer [16,17], using dimensional analysis and experimentally validated computer simulations. It was found that ignoring viscous dissipation could affect accurate flow simulations and measurements in microconduits. Aydin and Avci [8,9] have considered the effects of viscous heating in their studies. Viscous dissipation effect on fully developed slip flow forced convection in rectangular microchannels with constant wall heat flux has been studied by Aynor et al. [18]. Extended Graetz problem including viscous dissipation for a microtube was studied by Tunc and Bayazitoglu [19] using integral transform method. The two boundary conditions of constant wall temperature and constant wall heat flux were considered in the study. Similar study but for a slit microchannel with constant wall temperature was undertaken by Chen [20].

Entropy generation plays an important role in the design and development of thermofluid components. Entropy generation in the flow systems is due to fluid friction and heat transfer and it is increased by the presence of high gradients in velocity and temperature distributions. Such high gradients are found in very small scale devices such as microchannels. Entropy generation destroys available work of a system. Therefore, it makes good engineering sense to focus on irreversibility of heat transfer and fluid flow processes and try to understand the function of entropy generation mechanism. Bejan [21,22] focused on the different reasons behind entropy generation in applied thermal engineering. He showed that entropy minimization improves system efficiency. Nowadays, second law analysis of thermofluid systems has become a prominent topic in thermal engineering.

Although there are numerous works related to second law analysis of macroscale devices, unfortunately the open literature shows very small number of papers that deal with entropy generation in microdevices. It seems that Haddad et al. [23] were the first who performed the second law analysis for a microchannel. They numerically investigated the entropy generation due to developing laminar forced convection through parallel plate microchannels. Avci and Aydin [24] applied the second law analysis considering constant wall heat flux for two different microgeometries, namely, microtube and microducts, between two parallel plates. Hydrodynamically and thermally fully developed slip flow with constant properties was examined using the previously obtained velocity and temperature profiles. Hooman [25] presented closed form solutions for fully developed temperature distribution and entropy generation due to forced convection in the two above mentioned cross sections for two different thermal boundary conditions, being isothermal and isoflux walls. Recently, Sadeghi et al. [26] have performed the second law of thermodynamics analysis for steady state hydrodynamically and thermally fully developed laminar gas flow in annulus microchannels with constant wall heat fluxes.

The aim of the present study is to analytically investigate the entropy generation in extended Graetz problem including viscous dissipation in microtubes. The rarefaction effects are taken into consideration using first order slip boundary conditions. Using fully developed velocity profile, the energy equation is solved by means of integral transform. The interactive effects of rarefaction, viscous dissipation and the ratio of Brinkman number to dimensionless temperature difference on entropy generation rate and Bejan number are shown in graphical form and also discussed in detail.

NOMENCLATURE

Be	Bejan number [$= N_{HT}/N_S$]

Br	Brinkman number [$= \mu U^2/qR$]
c_p	specific heat at constant pressure [$\mathrm{kJkg^{-1}K^{-1}}$]
D_h	hydraulic diameter of channel [$= 2R$]
F	accommodation coefficient
h	heat transfer coefficient [$\mathrm{Wm^{-2}K^{-1}}$]
k	thermal conductivity [$\mathrm{Wm^{-1}K^{-1}}$]
Kn	Knudsen number [$= \lambda/D_h$]
N	normalization integral [Eq. (19)]
N_{FF}	entropy generation number related to fluid friction
N_{HT}	entropy generation number related to heat transfer
N_S	entropy generation number, total [$= S_G/S_{G,C}$]
$N_{S,av}$	average entropy generation number
Nu	Nusselt number [$= hD_h/k$]
p	pressure [Pa]
Pr	Prandtl number [$= \nu/\alpha$]
q	wall heat flux [$\mathrm{Wm^{-2}}$]
r	radial coordinate [m]
R	tube radius [m]
Re	Reynolds number [$= UD_h/\nu$]
S_G	entropy generation rate [$\mathrm{Wm^{-3}K^{-1}}$]
$S_{G,C}$	characteristic entropy generation rate [$\mathrm{Wm^{-3}K^{-1}}$]
T	temperature [K]
u	axial velocity [$\mathrm{ms^{-1}}$]
U	mean velocity [$\mathrm{ms^{-1}}$]
x	axial coordinate [m]

Greek Symbols

α	thermal diffusivity [$\mathrm{m^2s^{-1}}$]
β	eigenvalue
γ	heat capacity ratio
θ	dimensionless temperature [Eq. (8)]
λ	gas mean free path [m]
μ	dynamic viscosity [$\mathrm{kgm^{-1}s^{-1}}$]
ν	kinematic viscosity [$\mathrm{m^2s^{-1}}$]
φ	auxiliary variable [Eq. (12)]
Φ	transformed form of φ [Eq. (20)]
ψ	eigenfunction
Ω	dimensionless temperature difference [$= qR/kT_R$]

Subscripts

b	bulk
m	momentum
R	reference
s	fluid property at solid surface
t	thermal
w	wall
x	local
0	inlet
∞	fully developed flow property

Superscript

$*$	dimensionless variable

2 PROBLEM FORMULATION

2.1 Slip Velocity and Temperature Jump

As a result of slip velocity condition, the fluid particles adjacent to the solid surface no longer attain the velocity of the solid surface. Therefore, the fluid particles have a tangential velocity at the surface, which is the slip velocity, and it is expressed as [27]:

$$u_s = -\frac{2 - F_m}{F_m} Kn D_h \left(\frac{\partial u}{\partial r}\right)_w \tag{1}$$

where u_s is the slip velocity and F_m is the tangential momentum accommodation coefficient.

The fluid particles also have a finite temperature difference at the solid surface (temperature jump).Temperature jump is given by [27]

$$T_s - T_w = -\frac{2 - F_t}{F_t}\frac{2\gamma}{1+\gamma}\frac{Kn D_h}{Pr}\left(\frac{\partial T}{\partial r}\right)_w \tag{2}$$

where T_s is the temperature of the gas at the wall, T_w is the wall temperature and F_t is the thermal accommodation coefficient. The accommodation coefficients depend on various parameters that affect surface interaction, such as the magnitude and the direction of the velocity. It is shown that these coefficients are reasonably constant for a given gas and surface combination [28]. For many engineering applications the value of the accommodation coefficients are close to unity. For the rest of the analysis, F_m and F_t will be shown by F and assumed to be 1[13].

2.2 Hydrodynamic Aspects

Geometry of the physical problem is shown in Fig. 1. Flow is considered to be steady, hydrodynamically fully developed and having constant properties. Using coordinates shown in Fig. 1, the momentum equation in the x-direction is

$$\frac{1}{r}\frac{\mathrm{d}}{\mathrm{d}r}\left(r\frac{\mathrm{d}u}{\mathrm{d}r}\right) = \frac{1}{\mu}\frac{\mathrm{d}p}{\mathrm{d}x} = \text{constant} \tag{3}$$

and relevant boundary conditions are

$$u_{(R)} = -Kn D_h \left(\frac{\mathrm{d}u}{\mathrm{d}r}\right)_{(R)} = -2KnR\left(\frac{\mathrm{d}u}{\mathrm{d}r}\right)_{(R)} \tag{4a}$$

$$\left(\frac{\mathrm{d}u}{\mathrm{d}r}\right)_{(0)} = 0 \tag{4b}$$

Using dimensionless parameters, the dimensionless velocity distribution is

$$u^*(r^*) = 2\left(\frac{1+4Kn-r^{*2}}{1+8Kn}\right) \tag{5}$$

in which $r^* = r/R$, $u^* = u/U$ and U is the mean velocity.

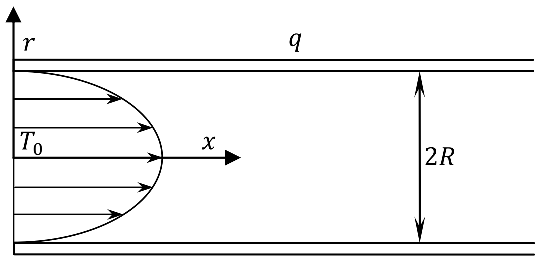

Fig. 1 Schematic of the physical problem and coordinate system.

2.3 First Law Analysis

It is assumed that temperature of the fluid entering the channel is uniform at $T = T_0$. Neglecting the axial conduction, the two dimensional energy equation in cylindrical coordinates may be written as

$$u\frac{\partial T}{\partial x} = \frac{\alpha}{r}\frac{\partial}{\partial r}\left(r\frac{\partial T}{\partial r}\right) + \frac{\nu}{c_p}\left(\frac{\mathrm{d}u}{\mathrm{d}r}\right)^2 \tag{6}$$

and relevant boundary conditions are

$$\left(\frac{\partial T}{\partial r}\right)_{(x,0)} = 0 \tag{7a}$$

$$k\left(\frac{\partial T}{\partial r}\right)_{(x,R)} = q \tag{7b}$$

$$T_{(0,r)} = T_0 \tag{7c}$$

In order to generalize the solution, the energy equation and relevant boundary conditions are made dimensionless, using the following dimensionless parameters, besides those introduced in section 2.2

$$\theta = \frac{T-T_0}{\frac{qR}{k}} \quad , \quad x^* = \frac{x}{RePrD_h} \tag{8}$$

The energy equation then is modified into the following dimensionless form

$$\frac{1+4Kn-r^{*2}}{2(1+8Kn)}\frac{\partial\theta}{\partial x^*} = \frac{1}{r^*}\frac{\partial}{\partial r^*}\left(r^*\frac{\partial\theta}{\partial r^*}\right) + \frac{16Br}{(1+8Kn)^2}r^{*2} \tag{9}$$

where the Brinkman number is defined as

$$Br = \frac{\mu U^2}{qR} \tag{10}$$

The Brinkman number is the criterion which shows the relative importance of viscous dissipation to the other terms of the energy equation. The thermal boundary conditions in the dimensionless form are written as

$$\left(\frac{\partial\theta}{\partial r^*}\right)_{(x^*,0)} = 0 \tag{11a}$$

$$\left(\frac{\partial\theta}{\partial r^*}\right)_{(x^*,1)} = 1 \tag{11b}$$

$$\theta_{(0,r^*)} = 0 \tag{11c}$$

Since the boundary conditions are non homogenous, therefore, we introduce a new variable φ, such that

$$\varphi(x^*,r^*) = \theta(x^*,r^*) - \theta_\infty(x^*,r^*) \tag{12}$$

where the fully developed temperature profile is simply derived as

$$\begin{aligned}\theta_\infty(x^*,r^*) = {} & \frac{c_1}{4}\left(r^{*2}-1\right) - \frac{c_2}{16}\left(r^{*4}-1\right) \\ & + c_3\left(\frac{c_1}{8}-\frac{c_2}{24}\right) - c_4\left(\frac{c_1}{24}-\frac{c_2}{64}\right) \\ & + 8\left[1+\frac{4Br}{(1+8Kn)^2}\right]x^*\end{aligned} \tag{13}$$

with

$$\left(\frac{\partial\theta_\infty}{\partial r^*}\right)_{(x^*,0)} = 0 \tag{14a}$$

$$\left(\frac{\partial\theta_\infty}{\partial r^*}\right)_{(x^*,1)} = 1 \tag{14b}$$

where

$$\begin{aligned} c_1 = {} & \frac{1+4Kn}{1+8Kn}\left[4+\frac{16Br}{(1+8Kn)^2}\right] \quad , \quad c_2 \\ & = \frac{4}{1+8Kn} + \frac{16Br}{(1+8Kn)^2} \\ & + \frac{16Br}{(1+8Kn)^3} \\ c_3 = {} & 2\frac{1+4Kn}{1+8Kn} \quad , \quad c_4 = \frac{2}{1+8Kn}\end{aligned} \tag{15}$$

The following equation system, which is obtained after the substitution of $\theta = \varphi + \theta_\infty$ into the energy equation, is satisfied by φ

$$\frac{1+4Kn-r^{*2}}{2(1+8Kn)}\frac{\partial\varphi}{\partial x^*} = \frac{1}{r^*}\frac{\partial}{\partial r^*}\left(r^*\frac{\partial\varphi}{\partial r^*}\right) \tag{16a}$$

$$\left(\frac{\partial\varphi}{\partial r^*}\right)_{(x^*,0)} = 0 \tag{16b}$$

$$\left(\frac{\partial\varphi}{\partial r^*}\right)_{(x^*,1)} = 0 \tag{16c}$$

$$\varphi_{(0,r^*)} = -\theta_{\infty(0,r^*)} \tag{16d}$$

The finite integral transform method [29], a straightforward and very general technique for the solution of Graetz type channel flow problems, is applied to solve the present heat transfer problem. To begin with, an integral transform pair is developed by considering an eigenvalue problem appropriate for the present problem. Next, by transformation, the partial derivative with respect to r^* is removed from Eq. (16a), reducing it to an ordinary differential equation. Then the resulting ODE is solved subject to the transformed initial condition. Finally, φ is immediately obtainable from the inversion formula. Based on the method of separation of variables, an appropriate eigenvalue problem is given by

$$\frac{1}{r^*}\frac{\mathrm{d}}{\mathrm{d}r^*}\left(r^*\frac{\mathrm{d}\psi}{\mathrm{d}r^*}\right) + \beta_m^2\left(1+4Kn-r^{*2}\right)\psi = 0 \tag{17a}$$

$$\left(\frac{\mathrm{d}\psi}{\mathrm{d}r^*}\right)_{(0)} = 0 \tag{17b}$$

$$\left(\frac{\mathrm{d}\psi}{\mathrm{d}r^*}\right)_{(1)} = 0 \tag{17c}$$

where $\psi(\beta_m, r^*)$'s and β_m's are the eigenfunctions and eigenvalues, respectively. Since the above eigenvalue problem constitutes a Sturm-Liouville problem, the eigenfunctions satisfy the following orthogonality condition

$$\int_0^1 r^*\left(1+4Kn-r^{*2}\right)\psi(\beta_m,r^*)\psi(\beta_n,r^*)\mathrm{d}r^* = \begin{cases} 0 & \text{for } m \neq n \\ N(\beta_m) & \text{for } m = n \end{cases} \tag{18}$$

where the normalization integral $N(\beta_m)$ is calculated from the following formula

$$N(\beta_m) = \int_0^1 r^*\left(1+4Kn-r^{*2}\right)[\psi(\beta_m,r^*)]^2\mathrm{d}r^* \tag{19}$$

Consequently, the integral transform pair with respect to the r^* variable is defined as

Transform:

$$\Phi(\beta_m,x^*) = \int_0^1 r^*\big(1+4Kn - r^{*2}\big)\psi(\beta_m,r^*)\varphi(x^*,r^*)\mathrm{d}r^* \tag{20}$$

Inversion:

$$\varphi(x^*,r^*) = \sum_{m=1}^{\infty}\frac{\psi(\beta_m,r^*)}{N(\beta_m)}\Phi(\beta_m,x^*) \tag{21}$$

The next step in the solution is solving the eigenvalue problem by the method of Frobenius. Assuming the function $\psi(\beta_m, r^*)$ to be a power series gives

$$\psi(\beta_m,r^*) = \sum_{j=0}^{\infty} a_j(\beta_m)r^{*j} \tag{22}$$

After substituting the above series into Eq. (17a) we obtain

$$a_1 = 0$$

$$a_2 = -\frac{\beta_m^2(1+4Kn)}{4}a_0$$

$$a_j = \begin{cases} 0 & \text{odd } j \geq 3 \\ \dfrac{\beta_m^2}{j^2}\left[a_{j-4} - a_{j-2}(1+4Kn)\right] & \text{even } j \geq 4 \end{cases} \tag{23}$$

a_0 will appear as an additive constant at all steps. Hence, without loss of generality, we can assume a_0 to be 1 as it will not affect the shape of the temperature profile and gradients at the wall. So, $\psi(\beta_m, r^*)$ and its derivative with respect to r^* can be written as

$$\psi(\beta_m,r^*) = 1 + a_2r^{*2} + a_4r^{*4} + \cdots \tag{24a}$$

$$\frac{\mathrm{d}\psi(\beta_m,r^*)}{\mathrm{d}r^*} = 2a_2r^* + 4a_4r^{*3} + \cdots \tag{24b}$$

From Eq. (24b), it is obvious that the first boundary condition of eigenvalue problem, Eq. (17b), is satisfied automatically. The second boundary condition is used to obtain eigenvalues. By substituting Eq. (24b) into Eq. (17c), we come up with

$$\sum_{j=2,4,\cdots}^{\infty} ja_j = 0 \tag{25}$$

Equation (25) may be rewritten by combining the coefficients of the terms containing the same power of β_m as

$$\sum_{k=1}^{\infty} b_k\beta^{2k} = b_1\beta^2 + b_2\beta^4 + \cdots = 0 \tag{26}$$

By numerically solving Eq. (26), the eigenvalues, β_m's are obtained. After solving the eigenvalue problem, we now take the integral transform of Eq. (16a) by the application of the transform (20). The transformation process starts with the operation on both terms of Eq. (16a) by the operator $\int_0^1 r^* \psi(\beta_m, r^*)\, dr^*$ to obtain

$$\frac{1}{2(1+8Kn)} \int_0^1 r^*\left(1+4Kn-r^{*2}\right) \psi(\beta_m, r^*) \frac{\partial \varphi}{\partial x^*} \mathrm{d}r^* = \int_0^1 \frac{\partial}{\partial r^*}\left(r^* \frac{\partial \varphi}{\partial r^*}\right) \psi(\beta_m, r^*) \mathrm{d}r^* \tag{27}$$

The term in the RHS of Eq. (27) is evaluated by integrating it by parts twice and utilizing the eigenvalue problem and the dimensionless boundary conditions of Eq. (16). Next, using the transform formula, we can obtain the following ordinary differential equation

$$\frac{\mathrm{d}\Phi_m}{\mathrm{d}x^*} + 2(1+8Kn)\beta_m^2 \Phi_m = 0 \tag{28}$$

The solution to Eq. (28) is given by

$$\Phi_m = A_m e^{-B_m x^*} \tag{29}$$

where

$$B_m = 2(1+8Kn)\beta_m^2 \tag{30}$$

and A_m which is the integral transformation of the initial condition has the following form

$$A_m = -\int_0^1 r^*\left(1+4Kn-r^{*2}\right)\left[\frac{c_1}{4}\left(r^{*2}-1\right) - \frac{c_2}{16}\left(r^{*4}-1\right) + c_3\left(\frac{c_1}{8}-\frac{c_2}{24}\right) - c_4\left(\frac{c_1}{24}-\frac{c_2}{64}\right)\right] \psi(\beta_m, r^*) \mathrm{d}r^* \tag{31}$$

Hence, the transformed temperature profile can be written as

$$\Phi_m = -\left\{\int_0^1 r^*\left(1+4Kn-r^{*2}\right)\left[\frac{c_1}{4}\left(r^{*2}-1\right) - \frac{c_2}{16}\left(r^{*4}-1\right) + c_3\left(\frac{c_1}{8}-\frac{c_2}{24}\right) - c_4\left(\frac{c_1}{24}-\frac{c_2}{64}\right)\right] \psi(\beta_m, r^*) \mathrm{d}r^*\right\} e^{-2(1+8Kn)\beta_m^2 x^*} \tag{32}$$

By introducing Eq. (32) into the inversion formula, $\varphi(x^*, r^*)$ becomes

$$\varphi(x^*, r^*) = -\sum_{m=1}^{\infty} \frac{\psi(\beta_m, r^*)}{\int_0^1 r^*(1+4Kn-r^{*2})[\psi(\beta_m, r^*)]^2 \mathrm{d}r^*} \left\{\int_0^1 r^*\left(1+4Kn-r^{*2}\right)\left[\frac{c_1}{4}\left(r^{*2}-1\right) - \frac{c_2}{16}\left(r^{*4}-1\right) + c_3\left(\frac{c_1}{8}-\frac{c_2}{24}\right) - c_4\left(\frac{c_1}{24}-\frac{c_2}{64}\right)\right] \psi(\beta_m, r^*) \mathrm{d}r^*\right\} e^{-2(1+8Kn)\beta_m^2 x^*} \tag{33}$$

Finally, the temperature distribution is obtained by adding θ_∞ to φ. Once the temperature distribution is obtained, the quantities of physical interest, including the bulk temperature of the fluid and the heat transfer rate can be obtained. The dimensionless bulk temperature can be expressed as

$$\theta_b = 2\int_0^1 u^*(r^*)\theta(x^*, r^*) r^* \mathrm{d}r^* \tag{34}$$

The heat transfer rate can be expressed in terms of the local Nusselt number as

$$Nu_x = \frac{h_x D_h}{k} = \frac{q D_h}{k(T_w - T_b)} = \frac{2}{\theta_s - \theta_b + \frac{4\gamma}{1+\gamma}\frac{Kn}{Pr}} \tag{35}$$

2.4 Second Law Analysis

Flow and heat transfer processes inside the microtube are irreversible. The non-equilibrium conditions arise due to the exchange of energy and momentum within the fluid and at solid boundaries, thus resulting in entropy generation. A part of the entropy production is due to the heat transfer in the direction of finite temperature gradients and the other part of entropy production arises due to the fluid friction. According to Bejan [22], the volumetric rate of entropy generation can be derived as

$$S_G = \frac{k}{T_R^2}\left(\frac{\partial T}{\partial r}\right)^2 + \frac{\mu}{T_R}\left(\frac{\mathrm{d}u}{\mathrm{d}r}\right)^2 \tag{36}$$

where T_R is the absolute reference temperature. Equation (36) can be made dimensionless to get entropy generation number N_S:

$$N_S = \frac{S_G}{S_{G,C}} = \left(\frac{\partial \theta}{\partial r^*}\right)^2 + \frac{Br}{\Omega}\left(\frac{\mathrm{d}u^*}{\mathrm{d}r^*}\right)^2 = N_{HT} + N_{FF} \tag{37}$$

where the dimensionless temperature difference Ω and the characteristic entropy generation rate $S_{G,C}$ are as follows

$$\Omega = \frac{qR}{kT_R} \tag{38a}$$

$$S_{G,C} = \frac{q^2}{kT_R^2} \tag{38b}$$

on the RHS of Eq. (37), N_{HT} represents entropy generation due to heat transfer and N_{FF} is the fluid friction contribution to entropy generation. Using dimensionless velocity and temperature distributions, entropy generation number becomes:

$$\begin{aligned} &N_S(x^*, r^*) \\ &= \left\{ -\sum_{m=1}^{\infty} \frac{\frac{\mathrm{d}\psi(\beta_m, r^*)}{\mathrm{d}r^*}}{\int_0^1 r^*(1+4Kn-r^{*2})[\psi(\beta_m, r^*)]^2 \mathrm{d}r^*} \left\{ \int_0^1 r^* \big(1 \right.\right. \\ &+ 4Kn - r^{*2}\big) \left[\frac{c_1}{4}\left(r^{*2}-1\right) - \frac{c_2}{16}\left(r^{*4}-1\right) + c_3\left(\frac{c_1}{8} - \frac{c_2}{24}\right) \right. \\ &\left.\left. - c_4\left(\frac{c_1}{24} - \frac{c_2}{64}\right)\right] \psi(\beta_m, r^*)\mathrm{d}r^* \right\} e^{-2(1+8Kn)\beta_m^2 x^*} + \frac{c_1}{2} r^* \\ &\left. - \frac{c_2}{4} r^{*3} \right\}^2 + \frac{16\frac{Br}{\Omega}}{(1+8Kn)^2} r^{*2} \end{aligned} \tag{39}$$

Note that $\partial\varphi/\partial r^*$ is damped at $x^* \to \infty$, so, the entropy generation number of fully developed flow $N_{S,\infty}$ will be in the following form

$$N_{S,\infty}(r^*) = \left(\frac{c_1}{2} r^* - \frac{c_2}{4} r^{*3}\right)^2 + \frac{16\frac{Br}{\Omega}}{(1+8Kn)^2} r^{*2} \tag{40}$$

The average dimensionless entropy generation over the cross section of the microchannel can be computed by the following integration

$$N_{S,av} = \frac{\int_0^1 N_S(x^*, r^*) r^* \mathrm{d}r^*}{\int_0^1 r^* \mathrm{d}r^*} = 2\int_0^1 N_S(x^*, r^*) r^* \mathrm{d}r^* \tag{41}$$

One of the irreversibility distribution parameters is the Bejan number Be, defined as the ratio of entropy generation due to heat transfer to total entropy generation rate, namely:

$$Be = \frac{N_{HT}}{N_S} \tag{42}$$

$Be = 1$ is the limiting value at which the heat transfer irreversibility dominates, while $Be = 0$ is the opposite limiting value where the irreversibility is solely attributable to fluid friction. Similar to entropy generation number, the fully developed Bejan number Be_∞ may be written as

$$Be_\infty(r^*) = \frac{\left(\frac{c_1}{2} r^* - \frac{c_2}{4} r^{*3}\right)^2}{\left(\frac{c_1}{2} r^* - \frac{c_2}{4} r^{*3}\right)^2 + \frac{16\frac{Br}{\Omega}}{(1+8Kn)^2} r^{*2}} \tag{43}$$

3 RESULTS AND DISCUSSION

Thermally developing slip flow through a micropipe is considered. Here, the interactive effects of Knudsen number, Brinkman number and the ratio of Brinkman number to dimensionless temperature difference on radial distribution of velocity and temperature and finally on entropy generation are analyzed. The results are presented for Kn ranging from 0.0 to 0.1, $Pr = 0.7$ and $\gamma = 1.4$. The procedure outlined in the previous section will be validated by comparing local Nusselt numbers with existing literature data.

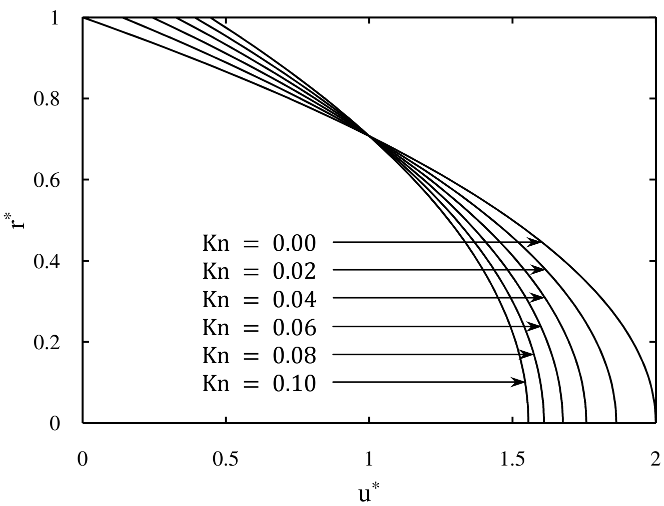

Fig. 2 Radial distribution of dimensionless velocity at different values of Knudsen number.

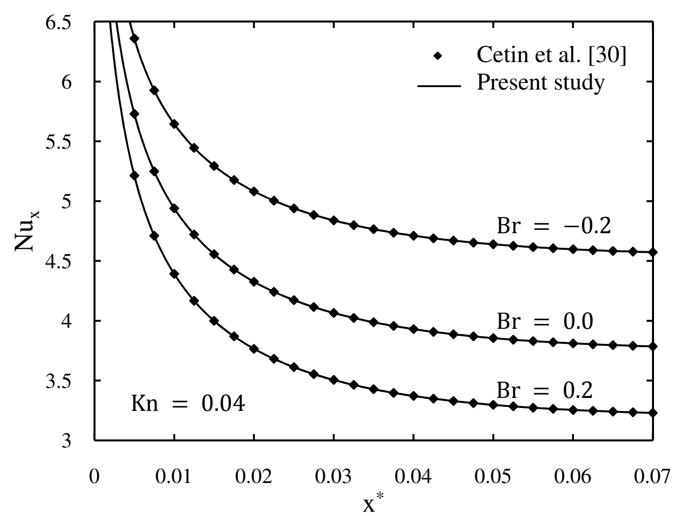

Fig. 3 Comparison between local Nusselt numbers obtained in present study against those given by Cetin et al. [30].

Figure 2 depicts radial distribution of dimensionless velocity at different values of Knudsen number. As a result of slip conditions, slip velocity occurs at the wall. An increase in Kn results in an increase in the slip velocity at the wall, while according to mass conservation, the maximum velocity decreases. Note that as Knudsen number increases the velocity gradient becomes smaller, especially at the wall at which the maximum decrease occurs. Figure 3 shows the comparison between local Nusselt numbers obtained in the present study against those given by Cetin et al. [30] for $Kn = 0.04$ at different values of Brinkman number. It should be noted that they numerically have solved energy equation using the finite difference scheme. As seen, there is an excellent agreement between the results.

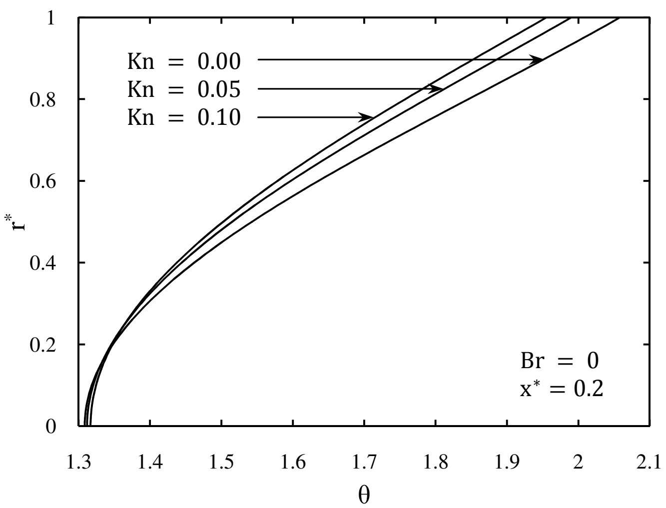

Fig. 4 Radial distribution of dimensionless temperature at different Knudsen numbers in the absence of viscous heating.

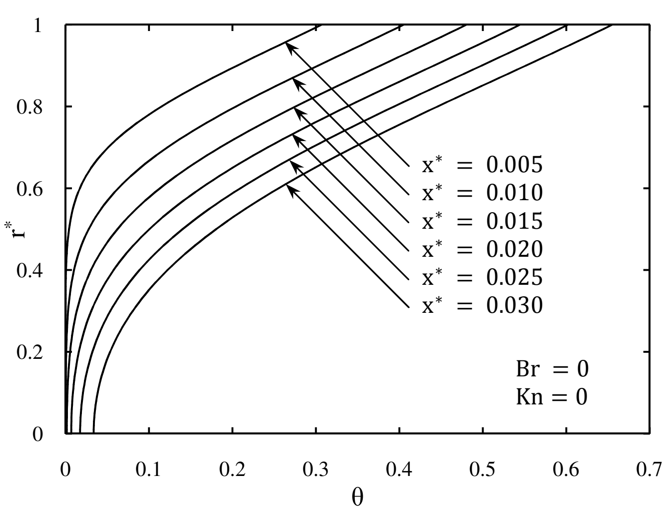

Fig. 5 Radial distribution of dimensionless temperature at different axial positions in the absence of viscous heating.

Radial distribution of dimensionless temperature of fully developed flow at different Knudsen numbers in the absence of viscous heating is illustrated in Fig. 4. As Knudsen number increases the dimensionless temperature decreases, with an exception of a small region adjacent to the centerline which it increases a little. In other words, slip conditions tend to unify the temperature distribution. Note that although the dimensionless temperature decreases over much of the duct cross section, the dimensionless bulk temperature remains unchanged. This is because the viscous heating is absent and the total energy delivered to the flow by the wall is not dependent on Knudsen number. Radial distribution of dimensionless temperature at different axial positions in the absence of viscous heating for no slip condition is presented in Fig. 5. As x^* increases the dimensionless temperature increases, which is an expected behavior. The existence of core flow which has not yet felt the presence of wall is seen for $x^* = 0.005$ and also at smaller regions for $x^* = 0.01$ and $x^* = 0.015$.

In Fig. 6 radial distribution of dimensionless temperature of fully developed flow at different values of Brinkman number is shown. Both positive and negative values of the wall heat flux are considered. Positive values of Brinkman number correspond to the wall cooling case at which heat is transferred from the wall to the fluid, while the opposite is true for negative values of Brinkman number. In the absence of viscous dissipation, the solution is independent of whether the wall is hot or cold. From the Figure, one can see that increasing values of Brinkman number lead to greater values of dimensionless temperature. This is due to the fact that as Brinkman number increases the energy generation due to viscous heating increases which this, consequently, increases the fluid temperature.

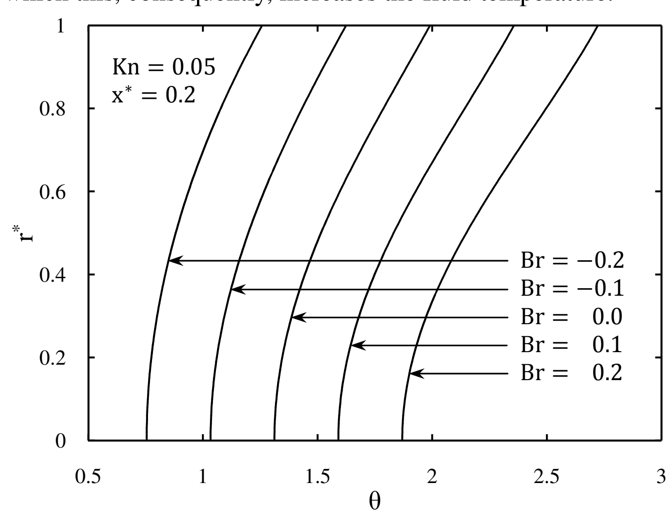

Fig. 6 Radial distribution of dimensionless temperature at different values of Brinkman number.

The main theme of the present work is to study entropy generation rate. Radial distribution of N_S for $Br = 0.2$, $Kn = 0.05$ and $Br/\Omega = 0.25$ at different axial positions is depicted in Fig. 7. The distribution of N_S at $x^* \to \infty$ has been obtained using Eq. (40). Entropy generation number attains its maximum value at the wall due to the presence of high velocity and temperature gradients. At centerline, at which velocity and temperature gradients are zero, the entropy generation number attains its minimum magnitude which is zero. As an expected behavior, the entropy generation number increases with increasing x^*. At the entrance the temperature distribution is uniform, except at the wall. So, the entropy generation is mainly due to fluid friction. As x^* is increased the extent of the core flow will shrink which this consequently leads to greater values of N_S. The corresponding Bejan number distribution for the above mentioned case is presented in Fig. 8. The Bejan number is greater for greater values of dimensionless axial coordinate. The Bejan number for $x^* = 0.005$ is zero in the vicinity of the centerline. This is the core flow which has not yet felt the presence of wall and the temperature is still uniform at T_0. For smaller values of x^* such as $x^* = 0.005$ and $x^* = 0.02$, the Bejan number attains its maximum value at a point close to the wall and reaches a local minimum at centerline, while for greater values of x^* the maximum and minimum values of Bejan number occur at centerline and the wall, respectively.

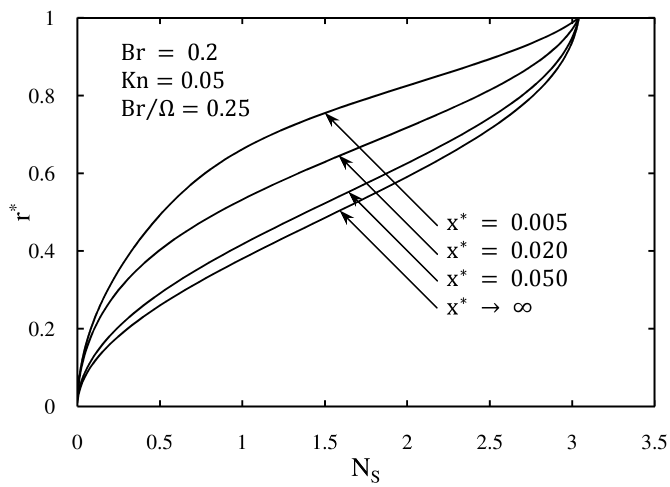

Fig. 7 Radial distribution of N_S at different axial positions.

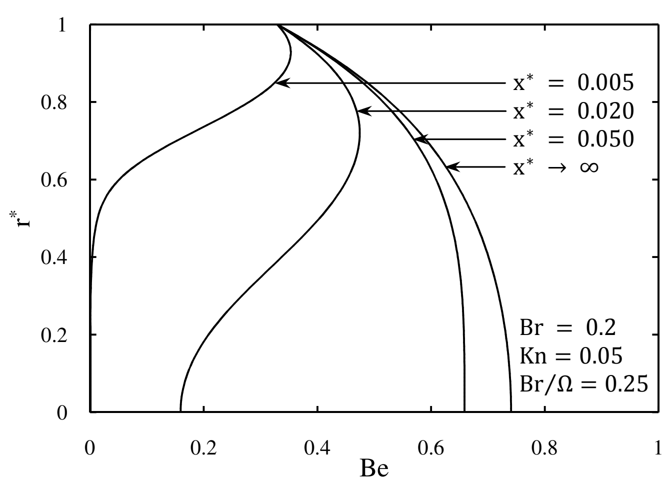

Fig. 8 Radial distribution of Bejan number at different axial positions.

Figure 9 illustrates radial distribution of $N_{S,\infty}$ for $Br = 0.2$ and $Br/\Omega = 0.25$ at different Knudsen numbers. Unless for $Kn = 0$, the maximum value of $N_{S,\infty}$ occurs at the wall. As Kn increases, the entropy generation is decreased due to decreasing the velocity and temperature gradients. The maximum decrement takes place at the wall at which the maximum decrement of velocity slope occurs. The corresponding Bejan number distribution for the above mentioned case is illustrated in Fig. 10. Increasing Knudsen number from 0 to 0.05 leads to greater values of Bejan number in the zone close to the wall which implies that the effect of Knudsen number on velocity distribution is greater than temperature distribution, while for the inner points it is vice versa. Greater Bejan numbers are achieved by increasing Kn from 0.05 to 0.1.

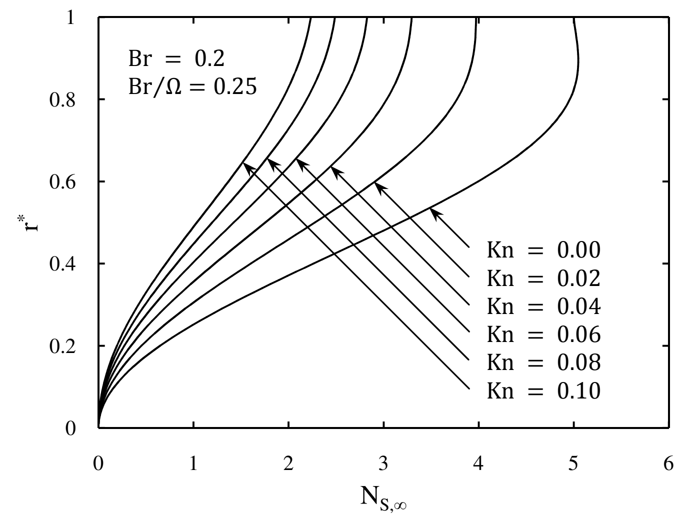

Fig. 9 Radial distribution of $N_{S,\infty}$ at different Knudsen numbers.

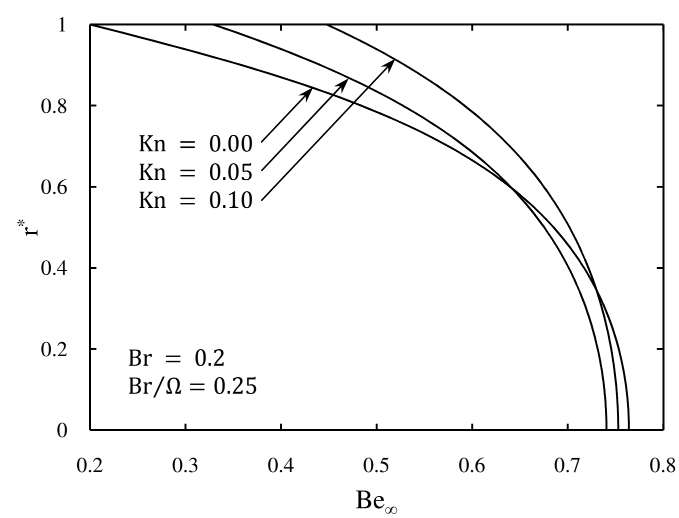

Fig. 10 Radial distribution of fully developed Bejan number at different Knudsen numbers.

Figure 11 shows radial distribution of $N_{S,\infty}$ for $Br = 0.2$ and $Kn = 0.05$ at different values of Br/Ω. As expected, increasing values of Br/Ω lead to greater values of $N_{S,\infty}$ due to increasing viscous effects. The maximum value of $N_{S,\infty}$ occurs at the wall, except for $Br/\Omega = 0$. In the absence of the fluid friction contribution to entropy generation, the point of maximum entropy generation number coincides with the point of maximum temperature gradient which for $Br = 0.2$ and $Kn = 0.05$ does not occurs at the wall. Radial distribution of fully developed Bejan number at different values of Br/Ω for $Br = 0.2$ and $Kn = 0.05$ is depicted in Fig. 12. For $Br/\Omega = 0$, the fluid friction contribution to entropy generation is zero. Bejan number is independent of radial coordinate and equal to its maximum value which is unity. For other values of Br/Ω, the maximum and minimum values of Bejan number occur at centerline and the wall, respectively. A greater Br/Ω leads to a smaller value of Bejan number due to increasing fluid friction effects.

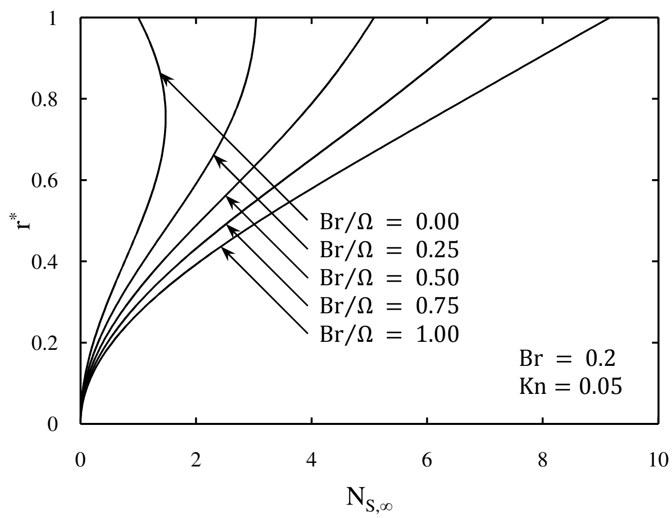

Fig. 11 Radial distribution of $N_{S,\infty}$ at different values of Br/Ω.

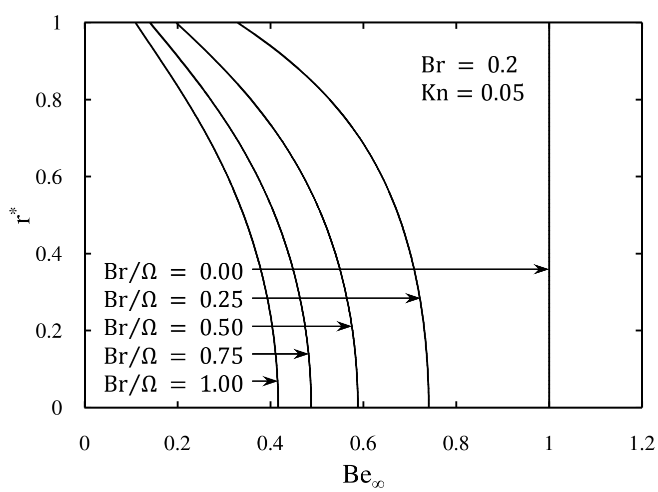

Fig. 12 Radial distribution of fully developed Bejan number at different values of Br/Ω.

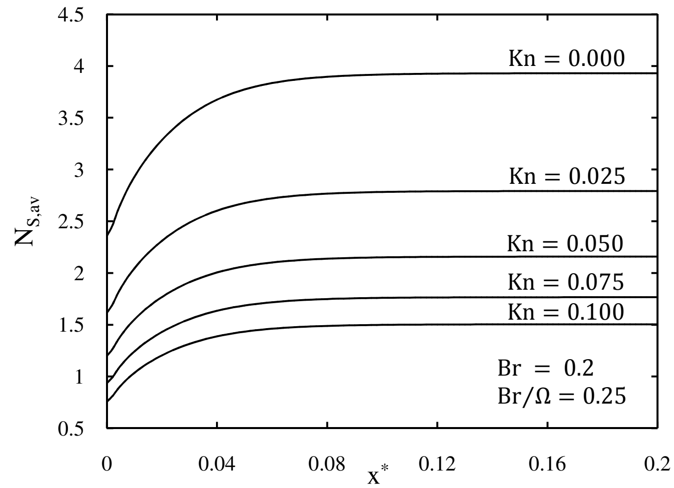

Fig. 13 Downstream variation of average entropy generation number at different Knudsen numbers.

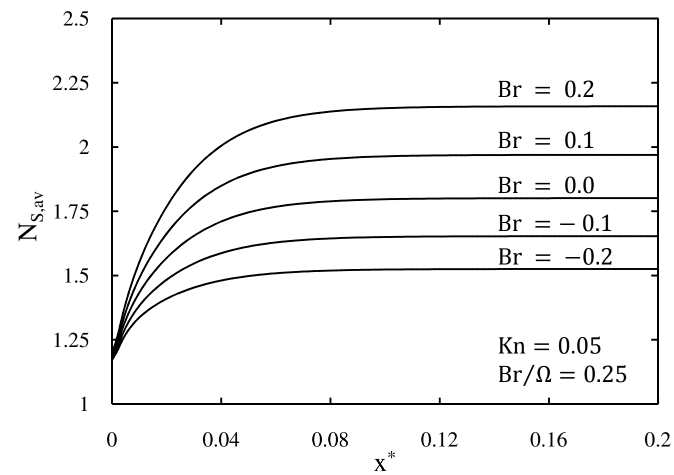

Fig. 14 Variation of average entropy generation number in the entrance region at different Brinkman numbers.

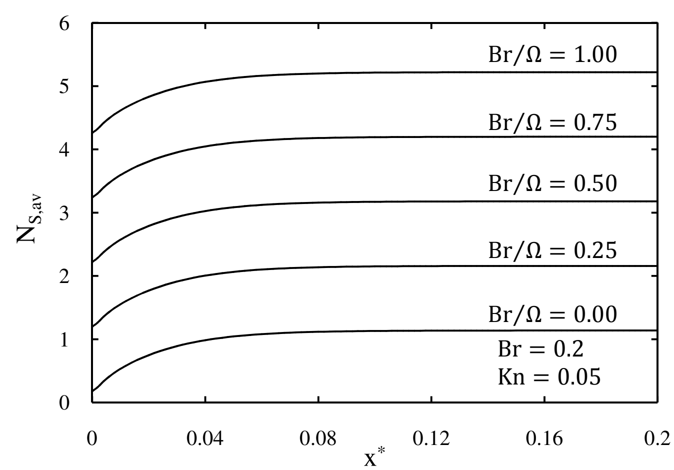

Fig. 15 Effects of Br/Ω on average entropy generation number in the entrance region.

Downstream variation of average entropy generation number at different Knudsen numbers for $Br = 0.2$ and $Br/\Omega = 0.25$ is presented in Fig. 13. It can be seen that to increase Knudsen is to decrease average entropy generation number due to decreasing temperature and velocity slopes. Also $N_{S,av}$ increases with increasing values of x^*, until it reaches a constant value at fully developed conditions. The reason is that as flow is thermally being developed the region affected by the wall heat flux will grow and consequently attain greater temperature gradients. Figure 14 shows variation of average entropy generation number in the entrance region at different Brinkman numbers for $Kn = 0.05$ and $Br/\Omega = 0.25$. A greater Brinkman number is accompanied by greater magnitudes of average entropy generation number, except at the entrance. At the entrance, entropy generation is mainly due to fluid friction effects and since viscous heating only affects temperature distribution, its effect on entropy generation is negligible. Effects of Br/Ω on average entropy generation number in the entrance region is illustrated in Fig. 15. Increasing Br/Ω results in greater magnitudes of $N_{S,av}$. The increment of average entropy generation number due to increasing values of Br/Ω is constant for each axial position. This is because of linear dependency of entropy generation to Br/Ω.

4 CONCLUSIONS

The second law of thermodynamics analysis has been carried out for extended Graetz problem in a microtube. The rarefaction effects as well as viscous heating effects were taken into consideration, but axial conduction was ignored. Using fully developed velocity profile, the energy equation was solved by means of integral transform. An expression for entropy generation number in the form of an infinite series was obtained. For fully developed conditions, closed form solutions were presented for entropy generation number and Bejan number. Some typical results of this study can be expressed as follows:

- The entropy generation decreases as Knudsen number increases. This is due to the fact that slip conditions tend to unify the velocity and temperature profiles.
- The effect of increasing values of Brinkman number and the ratio of Brinkman number to dimensionless temperature difference is to increase entropy generation.
- The average entropy generation number over the cross section of channel increases with increasing values of axial coordinate, until it reaches a constant value at fully developed conditions.

5 REFERENCES

[1] Harley, J., Huang, Y., Bau, H., and Zemel, J.N., 1995, "Gas Flow in Microchannels," *J. Fluid Mech.*, 284, pp. 257–274.

[2] Araki, T., Kim, M.S., Hiroshi, I. and Suzuki, K., 2000, "An Experimental Investigation of Gaseous Flow Characteristics in Microchannels," *G.P. Celata, et al. (Eds.), Proceedings of International Conference on Heat Transfer and Transport Phenomena in Microscale*, Begell House, New York, USA, pp. 155–161.

[3] Beskok, A., and Karniadakis, G.E., 1994, "Simulation of Heat and Momentum Transfer in Complex Micro-Geometries," *J. Thermophysics Heat Transfer*, 8, pp. 647–655.

[4] Kennard, E.H., 1938, *Kinetic Theory of Gases*, McGraw–Hill, New York.

[5] Ebert, W.A., and Sparrow, E.M., 1965, "Slip Flow in Rectangular and Annular Ducts," *J. Basic Engrg.*, 87, pp. 1018–1024.

[6] Duan, Z., and Muzychka, Y.S., 2007, "Slip Flow in Elliptic Microchannels," *Int. J. Therm. Sci.*, 46, pp. 1104–1111.

[7] Zhu, X., Xin, M.D., and Liao, Q., 2002, "Analysis of Heat Transfer Between Two Unsymmetrically Heated Parallel Plates With Microspacing in the Slip Flow Regime," *Microscale Thermophys. Eng.*, 6, pp. 287–301.

[8] Aydin, O., and Avci, M., 2006, "Heat and Flow Characteristics of Gases in Micropipes," *Int. J. Heat Mass Transfer*, 49, pp. 1723–1730.

[9] Aydin O., and Avci M., 2007, "Analysis of Laminar Heat Transfer in Micro-Poiseuille Flow, *Int. J. Therm. Sci.*, 46, pp. 30–37.

[10] Duan, Z., and Muzychka, Y.S., 2008, "Slip Flow Heat Transfer in Annular Microchannels With Constant Heat Flux," *J. Heat Transfer*, 130(9), 092401.

[11] Ghodoossi, L., and Egrican, N., 2005, "Prediction of Heat Transfer Characteristics in Rectangular Microchannels for Slip Flow Regime and H1 Boundary Condition," *Int. J. Therm. Sci.*, 44, pp. 513–520.

[12] Graetz, L., part 1, 1883, part 2, 1885, "Uber die Warmeleitungsfahigheit von Flussingkeiten," *Annalen der Physik und Chemie*, part 1, 18, pp. 79–94, part 2, 25, pp. 337–357.

[13] Barron, R.F., Wang, X., Ameel, T.A., and Warrington, R.O., 1997, "The Graetz Problem Extended to Slip Flow," *Int. J. Heat Mass Transfer*, 40, 8, pp. 1817-1823.

[14] Ameel, T.A., Wang, X.M., Baron, R.F., and Warrington, R.O., 1997, "Laminar Forced Convection in a Circular Tube With Constant Heat Flux and Slip Flow," *Microscale Thermophys. Eng.*, 1(4), pp. 303–320.

[15] Yu, S., and Ameel, T.A., 2001, "Slip Flow Heat Transfer in Rectangular Microchannels," *Int. J. Heat Mass Transfer*, 44, pp. 4225–4234.

[16] Koo, J., and Kleinstreuer, C., 2004, "Viscous Dissipation Effects in Microtubes and Microchannels," *Int. J. Heat Mass Transfer*, 47, pp. 3159–3169.

[17] Koo, J., and Kleinstreuer, C., 2003, "Liquid Flow in Microchannels: Experimental Observations and Computational Analyses of Microfluidics Effects," *J. Micromechanics and Microengineering*, 13, pp. 568–579.

[18] Aynur, T.N., Kuddusi, L., and Egrican, N., 2006, "Viscous Dissipation Effect on Heat Transfer Characteristics of Rectangular Microchannels Under Slip Flow Regime and

H1 Boundary Conditions," *Heat Mass Transfer*, 42, pp. 1093–1101.

[19] Tunc, G., and Bayazitoglu, Y., 2001, "Heat Transfer in Microtubes With Viscous Dissipation," *Int. J. Heat Mass Transfer*, 44, pp. 2395–2403.

[20] Chen, C.H., 2006, "Slip Flow Heat Transfer in a Microchannel With Viscous Dissipation," *Heat Mass Transfer*, 42, pp. 853–860.

[21] Bejan, A., 1982, "Second Law Analysis in Heat Transfer and Thermal Design," *Advances in Heat Transfer*, 15, pp. 1–58.

[22] Bejan, A., 1996, *Entropy Generation Minimization*, CRC Press, New York.

[23] Haddad, O., Abuzaid, M., and Al-Nimr, M., 2004, "Entropy Generation due to Laminar Incompressible Forced Convection Flow Through Parallel Plates Microchannel," *Entropy*, 6, 5, pp. 413–426.

[24] Avci, M. and Aydin, O., 2007, "Second Law Analysis of Heat and Fluid Flow in Microscale Geometries," *Int. J. Exergy*, 4, 3, pp. 286–301.

[25] Hooman, K., 2007, "Entropy Generation for Microscale Forced Convection: Effects of Different Thermal Boundary Conditions, Velocity Slip, Temperature Jump, Viscous Dissipation, and Duct Geometry," *Int. Comm. Heat Mass Transfer*, 34, pp. 945–957.

[26] Sadeghi, A., Asgarshamsi, A., and Saidi, M.H., 2009, "Second Law Analysis of Slip Flow Heat Transfer in Annulus Microchannel," *Proceedings of ASME Summer Heat Transfer Conference*, San Francisco, California.

[27] Beskok, A., Karniadakis, G.E., and Trimmer, W., 1996, "Rarefaction and Compressibility Effects in Gas Microflows," *J. Fluids Engrg.*, 118, pp. 448–456.

[28] Schaaf, S.A., 1963, "Mechanics of Rarefied Gases," Encyclopedia of Physics, Vol. Fluid Dynamics II, VII/2, Berlin, pp. 591–624.

[29] Bayazitoglu, and Y., Ozisik, M.N., 1980, "On the Solution of Graetz Type Problems With Axial Condition," *Int. J. Heat Mass Transfer*, 23, pp. 1399–1402.

[30] Cetin, B., Yuncu, H., and Kakac, S., 2006 "Gaseous Flow in Microconduits With Viscous Dissipation, *Int. J. Trans. Phenomena*, 8, pp. 297–315.

